ARL-TR-10242 ● Dec 2025

Parametric Study of Americium Thickness for Alphavoltiac Device Electrical Power Optimization

by Benjamin Cohen, Owen Li, and Marc Litz

NOTICES

Disclaimers

ARL-TR-10242 ● DEC 2025

Parametric Study of Americium Thickness for Alphavoltiac Device Electrical Power Optimization

Benjamin Cohen
University of Maryland, National Security Scholars Summer Internship Program

Owen Li
United States Military Academy, Advanced Individual Development Program

Marc Litz
DEVCOM Army Research Laboratory

REPORT DOCUMENTATION PAGE

1. REPORT DATE	2. REPORT TYPE	3. DATES COVERED START DATE	3. DATES COVERED END DATE
December 2025	Technical Report	6/1/2025	8/31/2025

4. TITLE AND SUBTITLE
Parametric Study of Americium Thickness for Alphavoltiac Device Electrical Power Optimization

5a. CONTRACT NUMBER	5b. GRANT NUMBER	5c. PROGRAM ELEMENT NUMBER

5d. PROJECT NUMBER	5e. TASK NUMBER	5f. WORK UNIT NUMBER

6. AUTHOR(S)
Benjamin Cohen, Owen Li, and Marc Litz

7. PERFORMING ORGANIZATION NAME(S) AND ADDRESS(ES)	8. PERFORMING ORGANIZATION REPORT NUMBER
DEVCOM Army Research Laboratory ATTN: FCDD-RLA-GC Adelphi, MD 20783	ARL-TR-10242

9. SPONSORING/MONITORING AGENCY NAME(S) AND ADDRESS(ES)	10. SPONSOR/MONITOR'S ACRONYM(S)	11. SPONSOR/MONITOR'S REPORT NUMBER(S)

12. DISTRIBUTION/AVAILABILITY STATEMENT
DISTRIBUTION STATEMENT A. Approved for public release: distribution unlimited.

13. SUPPLEMENTARY NOTES

14. ABSTRACT
Alphavoltaic (AV) energy conversion, in which an alpha particle flux from radioisotope sources such as ^{241}Am is converted into electrical power, offers the promise of a higher power output as compared to the more established betavoltaic systems. First, a comparison of beam and layer geometry into aluminum gallium nitride (AlGaN) is described. The beam-delivered alphas describe experimental configurations using a Pelletron accelerator while a layer of americium (Am) deposited on a 1-cm^2 energy converter describes final use configuration. We investigate the geometry (layer thickness) of ^{241}Am to maximize power transferred into the semiconductor target (AlGaN) describing an AV persistent power source. Identical studies were conducted for pure Am as a foil, AmO_2, $AmCl_3$, $Am(NO_3)_3$ for comparison. Alpha particles exposing AlGaN semiconductor structures generate electron hole pairs creating a continuous and persistent trickle charge of electrical power. Pure ^{241}Am foil provides the highest power into the AlGaN at 10.37-µm source thickness. Most AlGaN diodes have an active charge collection of 2 µm. AmO_2 with a thickness of 6.96 µm delivers 68 µW to the active charge collection depth (first 2 µm) of AlGaN.

15. SUBJECT TERMS
alphavoltaic, AV, power conversion, americium, aluminum gallium nitride, AlGaN, Monte-Carlo N Particle, MCNP, Energy Sciences

16. SECURITY CLASSIFICATION OF: a. REPORT	b. ABSTRACT	C. THIS PAGE	17. LIMITATION OF ABSTRACT	18. NUMBER OF PAGES
UNCLASSIFIED	UNCLASSIFIED	UNCLASSIFIED	UU	29

19a. NAME OF RESPONSIBLE PERSON	19b. PHONE NUMBER *(Include area code)*
Marc Litz	(520) 691-6193

STANDARD FORM 298 (REV. 5/2020)
Prescribed by ANSI Std. Z39.18

Contents

List of Figures **iv**

List of Tables **v**

1. Introduction **1**

2. Modeling and Simulation Approach **3**

3. Results and Discussion **4**

4. Conclusion **10**

5. References **12**

Appendix A. Monte-Carlo N Particle (MCNP) Input Deck of 10-µm-thick Americium (Am) Source **13**

Appendix B. Energy Deposition Tables **17**

List of Symbols, Abbreviations, and Acronyms **21**

Distribution List **22**

List of Figures

Figure 1. AlGaN has a high bandgap and low lattice constant, meaning it has a very structurally sound lattice and is more resistant to radiation than commonly used semiconductor materials like gallium nitride (GaN) and silicon carbide (SiC).. 2

Figure 2. (a) Schematic drawing of radioisotope layer surrounded by AlGaN energy converter. The 1- × 1-cm × varying radioisotope layer width is modelled. (b) The geometry of the input deck varies the radioisotope layer from 2 to 26 µm thick. 3

Figure 3. Energy deposition (a) mesh contour plot and (b) graph of alphas and secondary electrons for the 10-µm-thick ^{241}Am source coupled with AlGaN. 4

Figure 4. Alpha (dashed) and electron (dotted) energy deposition as a function of range into AlGaN is shown for a 10-µm-thick radioisotope layer. 87% and 13% are the energy losses from alpha and secondary electrons, respectively. The $AmCl_3$ and $Am(NO_3)_3$ secondary electron energy deposition curves overlap... 5

Figure 5. Simulated source efficiency at various radioisotope widths for each Am compound studied. 6

Figure 6. Shows the linear relationship between radioisotope width and activity (1 mCi = 3.7 × 10^7 decay/s). This is dependent on specific activity and material density (which can be found in Table 1) and cross-sectional geometry of the source. 7

Figure 7. Power deposited in one side of the AlGaN (red) and first 2 µm of the AlGaN (blue) shown for each radioisotope studied............................. 8

Figure 8. Power deposition in the first 2 µm of the AlGaN transducer as a function of radioisotope width for each Am compound studied. Saturation width and power are marked. 9

Figure 9. Schematic design of APV device <175 µm thick. 11

List of Tables

Table 1. 90% saturation width for each Am compound studied. 9

Table 2. Double-sided AV device specifications based on 90% saturation width. 10

Table 3. EHP generation rate in the first 2 μm of AlGaN. 10

Table B-1. Am alpha data. 19

Table B-2. AmO_2 alpha data. 19

Table B-3. $AmCl_3$ alpha data. 20

Table B-4. $Am(NO_3)_3$ alpha data. 20

1. Introduction

Nuclear-powered devices offer a viable solution for applications where high-power density and operational lifetime are needed. This is useful for industrial sensing and space applications where devices and sensors must often be remote, lightweight, and miniature. However, before deploying nuclear power sources to support electronic devices, it is important for the radiation effects to be thoroughly investigated to ensure optimized performance and longevity.

In this study, we explore various thicknesses for ^{241}Am, a commercially available radioisotope commonly used in smoke sensors and density moisture tools. Americium (Am) foils and the compounds AmO_2, $AmCl_3$, and $Am(NO_3)_3$ are compared in terms of energy coupled into an aluminum gallium nitride (AlGaN) energy converter. Am is an alpha-emitting radioisotope of interest due to its 5.5-MeV emission and 432-year half-life. The lifetime of the power converter is limited by the degradation of the energy converter because of the alpha mass and kinetic energy.

AlGaN is considered a radiation tolerant material based on its large bandgap and small lattice constant. AlGaN exhibits a small decrease in drain current with increasing fluence of protons in HEMT (High Electron Mobility Transistor) devices, meaning it has a high displacement energy and is very radiation tolerant (Weaver et al. 2012). This material property is likely present in vertical voltaic devices as well. It has also been theorized that AlGaN's strong piezoelectric effect causes scattered carriers to be reinjected to the conduction area (2DEG region), inhibiting destructive mechanisms (Weaver et al. 2016). Ultimately, AlGaN showed impressive resistance to high-energy alpha-induced device degradation, making it useful for long-lived alpha energy conversion applications (Figure 1).

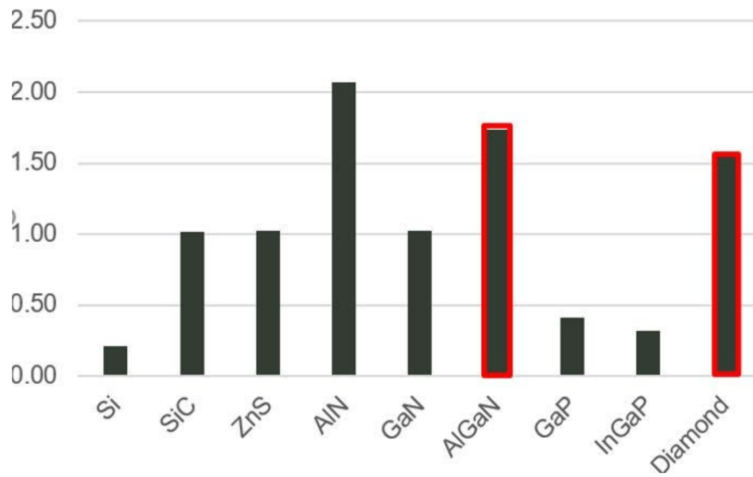

Figure 1. AlGaN has a high bandgap and low lattice constant, meaning it has a very structurally sound lattice and is more resistant to radiation than commonly used semiconductor materials like gallium nitride (GaN) and silicon carbide (SiC).

Radioisotope layer thickness is an important design consideration that dictates both power output and source efficiency. Power output can be expressed as the power released by radiation from the radioisotope multiplied by a long string of conversion efficiencies:

$$P_{out}=P_{source}\,\eta_{src}\,\eta_{cpl}\,\eta_{EC}$$

Thus, meaning a higher source power is correlated with a higher power output (Olsen 1993). Activity is given by the radioisotope's characteristic specific activity, measured in Ci/g and multiplied by its mass. From this, we get the following equation for activity of a radioisotope film:

$$A = A_{sp}V\rho$$

where A is activity, A_{sp} is specific activity, V is radioisotope volume, and ρ is radioisotope density. There is, however, a limit to the power deposited in the energy converter based on the radioisotope geometry. Although both activity and power released increase with source thickness, the finite range of the alpha limits energy deposited into the converter and the alphas emitted from deep within the source will often not contribute to power conversion in the semiconductor. Furthermore, increased radioisotope width correlates with lower gravimetric and volumetric power density.

In addition to radioisotope width, energy deposition as a function of range is important for creating a "well-matched" design (Prelas et al. 2014). For energy conversion to occur in AlGaN, carrier charges must be generated in the depletion zone—i.e., the region between where the magnesium (Mg) P-doped and silicon (Si) N-doped regions meet (Van de Walle et al. 1999). The difference in donor/acceptor concentrations creates a built-in electric field to carry the freed electron and holes and create current.

2. Modeling and Simulation Approach

To simulate the radioisotope's energy deposition in AlGaN, both Monte-Carlo N Particle (MCNP) and Stopping Range in Matter (SRIM) were used. MCNP is a general-purpose radiation transport code that was used to simulate the interaction of alphas and electrons with matter used for volumetric source modeling. SRIM is a group of programs that simulates how ions interact with matter used to confirm properties of the radioisotopes studied. In our first iteration of the simulation, we used MCNP to compare the results of a 5.5-MeV beam source versus a 1-cm × 1-cm × 2-μm 5.5-MeV volumetric source. The beam source was used as a practical way to measure the effects of an alpha particle into the semiconductor.

For the volumetric source simulation, we varied each of the ^{241}Am radioisotope compound widths from 2 to 26 μm with a step size of 2 μm, making the total number of simulations per compound 13. The basic geometry for the volumetric source is shown in Figure 2.

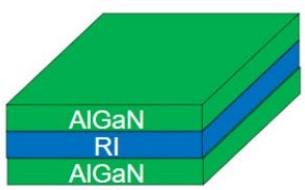

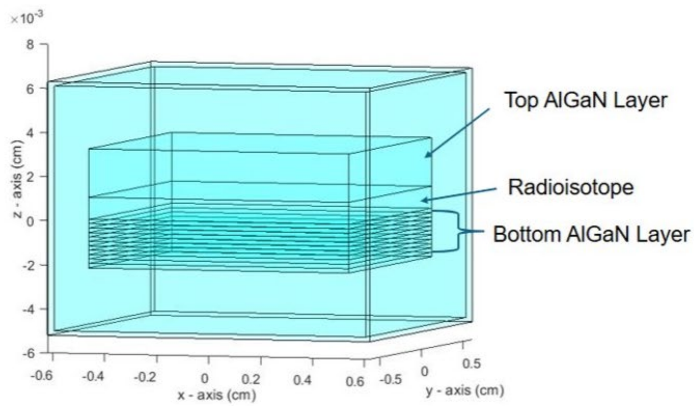

(a) (b)

Figure 2. (a) Schematic drawing of radioisotope layer surrounded by AlGaN energy converter. The 1- × 1-cm × varying radioisotope layer width is modelled. (b) The geometry of the input deck varies the radioisotope layer from 2 to 26 μm thick.

Tallies in MCNP were used to score the alpha and electron energy and flux in every cell, which included the radioisotope compound. The mesh function was used to visualize the energy deposition and flux. The complete MCNP input deck describing material cells as well as particle energy deposition reactions is shown in Appendix A. A total of 250,000 particles were tracked in each simulation. MATLAB software was used to visualize the geometry and tally and mesh data.

3. Results and Discussion

To ensure our results were accurate and all energy was tracked, a conservation of energy calculation was conducted for all simulations. All alpha and electron energy deposited in the device and surroundings per particle was within 0.1% of 5.5 MeV (energy of the sourced α particle), concluding that all energy (with the exception of <5 keV) was accounted for in the simulation.

A 2-µm layer of Am sandwiched between two AlGaN layers and a 5.5-MeV beam shot into AlGaN is shown in Figure 3 for comparison. The contour plots quantify the energy deposition from alphas and secondary electrons. The energy deposition in each of the 100-nm defined layers of the AlGaN is tabulated in Appendix B. The secondary electrons are created from the ionization energy lost by alphas. The range is taken as the penetration depth at which the energy deposited (MeV/cc) is 10% of the initial kinetic energy. The range of alphas and secondary electrons are shown to be 10.2 and 3.7 µm, respectively, for the volumetric alpha source, and 13.3 and 9.8 µm, respectively, for the alpha beam. This difference in particle range emphasizes that measurements taken from an alpha beam will not duplicate the energy deposition from the isotropic emission of a radioisotope layer. Another difference observed is the initial energy deposition is larger for the beam than the radioisotope layer because there is already some energy lost by the alpha due to self-shielding from the 2-µm Am layer.

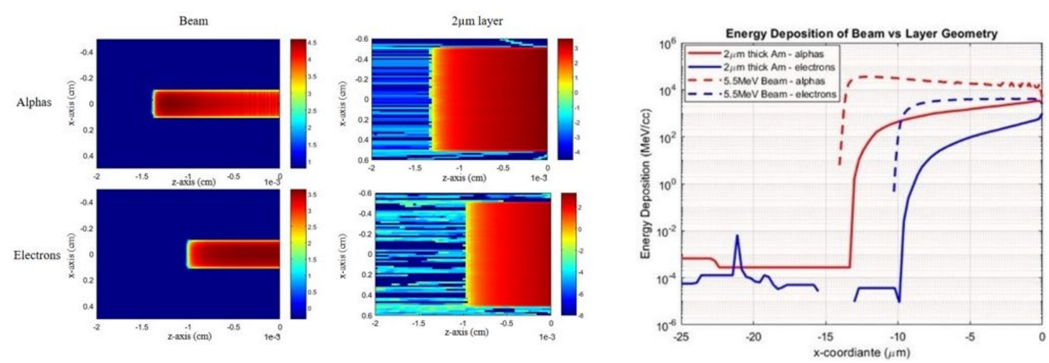

(a) (b)

Figure 3. Energy deposition (a) mesh contour plot and (b) graph of alphas and secondary electrons for the 10-µm-thick ^{241}Am source coupled with AlGaN.

The partitions of energy deposition from alphas are compared to that of secondary electrons. The combination of alpha and electron energy deposited agrees with the total energy of 5.5 MeV per source particle; 87% of energy deposited comes from alpha energy loss and the other 13% goes into generating secondary electrons. The energy breakdown of alpha and electron energy is shown for comparison of alphas and secondary electron energy in Figure 4.

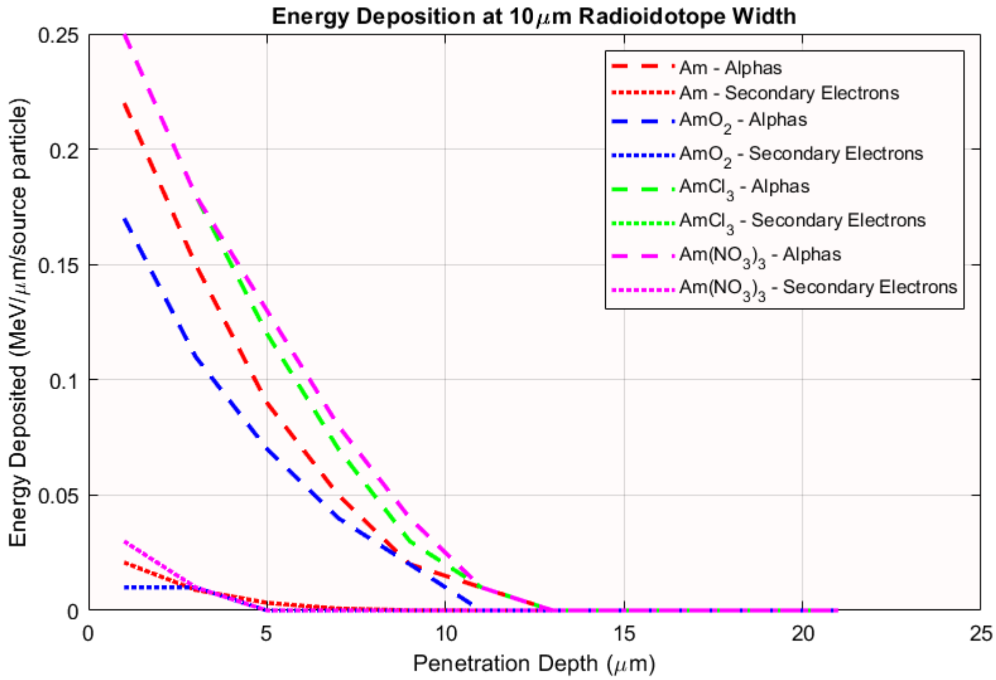

Figure 4. Alpha (dashed) and electron (dotted) energy deposition as a function of range into AlGaN is shown for a 10-µm-thick radioisotope layer. 87% and 13% are the energy losses from alpha and secondary electrons, respectively. The $AmCl_3$ and $Am(NO_3)_3$ secondary electron energy deposition curves overlap.

Source efficiency is defined as the percent of energy deposition in the semiconductor compared to the total energy emitted by the radioisotope per decay (Olsen 1993). The source efficiency is just one in the string of efficiencies to estimate the net betavoltaic efficiency. To calculate the source efficiency, the tally of energy deposition per gram in each of the semiconductor cells calculated by MCNP was used. This ratio can also be applied to find the power deposited in the AlGaN compared to the source power. Figure 5 shows the source efficiency as a function of the radioisotope layer thickness for each Am compound studied.

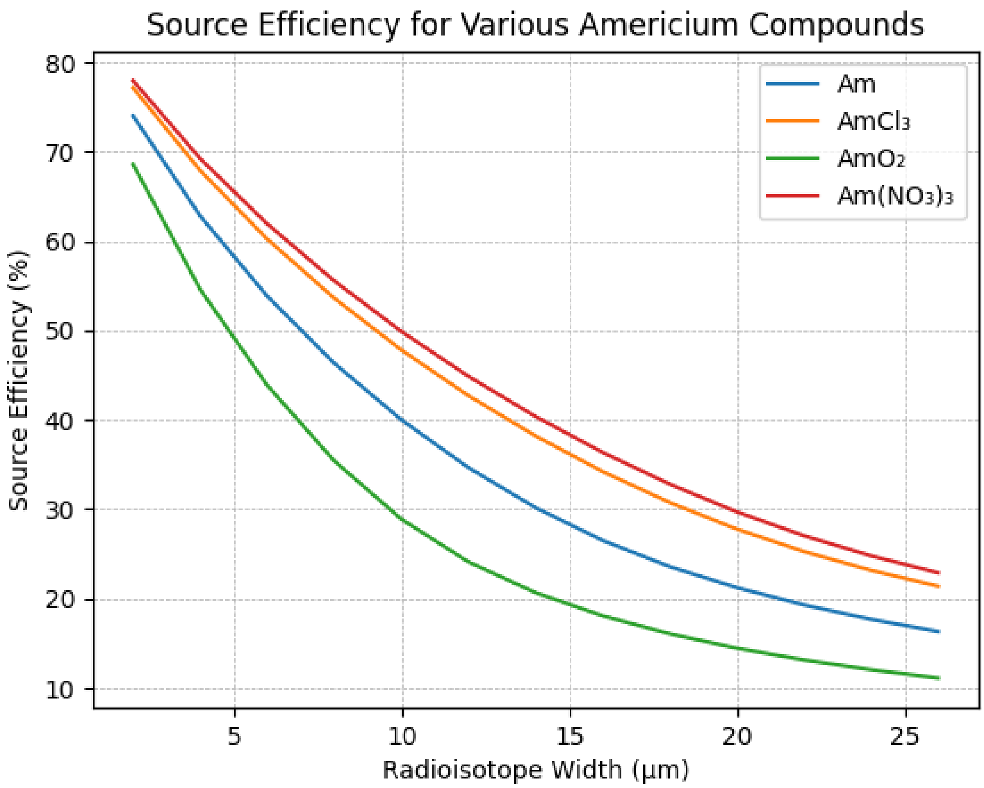

Figure 5. Simulated source efficiency at various radioisotope widths for each Am compound studied.

Source efficiency decreases with increasing radioisotope layer thickness due to more self-absorption within the material. Particles that are self-absorbed fail to deposit energy in the semiconductor and therefore do not contribute to power generation, resulting in reduced overall efficiency. The average range of an emitted ion increases as material density decreases, making self-absorption less significant in lower-density materials. See Table 1 (density values). This trend is observed in Figure 5, where source efficiency declines with density with the exception of AmO_2.

Source efficiency describes the proportion of energy removed from the source; however, we aim to optimize electrical power output. As the radioisotope width increases, source efficiency decreases. However, activity is increasing proportional to its mass, leading to a higher maximum electrical power output. Figure 6 shows the linear relationship between radioisotope width and source activity.

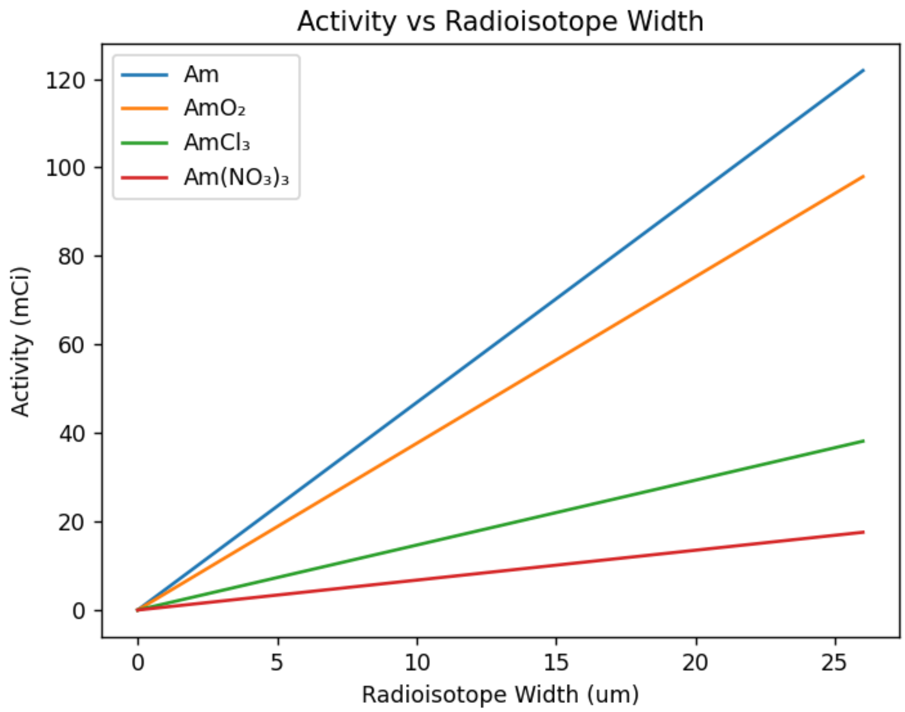

Figure 6. Shows the linear relationship between radioisotope width and activity (1 mCi = 3.7×10^7 decay/s). This is dependent on specific activity and material density (which can be found in Table 1) and cross-sectional geometry of the source.

In maximizing the electrical power output, the source width is varied. The energy deposition in the first 2 µm, as well as in one side of the AlGaN, are quantified. Energy deposition in the first 2 µm is more relevant for direct power conversion compared to the full AlGaN semiconductor because the depletion region of an AlGaN PIN junction is largely within the first 2 µm. If the electron hole pairs (EHPs) are created outside the electric field of the PIN junction, they have a high likelihood of recombining with the medium and not being converted to an electrical current. The specifics of the depletion layer are not within the scope of this study, considering the energy deposited near the depletion zone is important for optimizing power output in an alphavoltaic (AV) device. Curves for power delivered by the source as well as power deposited in the first 2 µm and one side are shown in Figure 7. The first 2 µm absorbs approximately 40% of the energy deposited in the AlGaN.

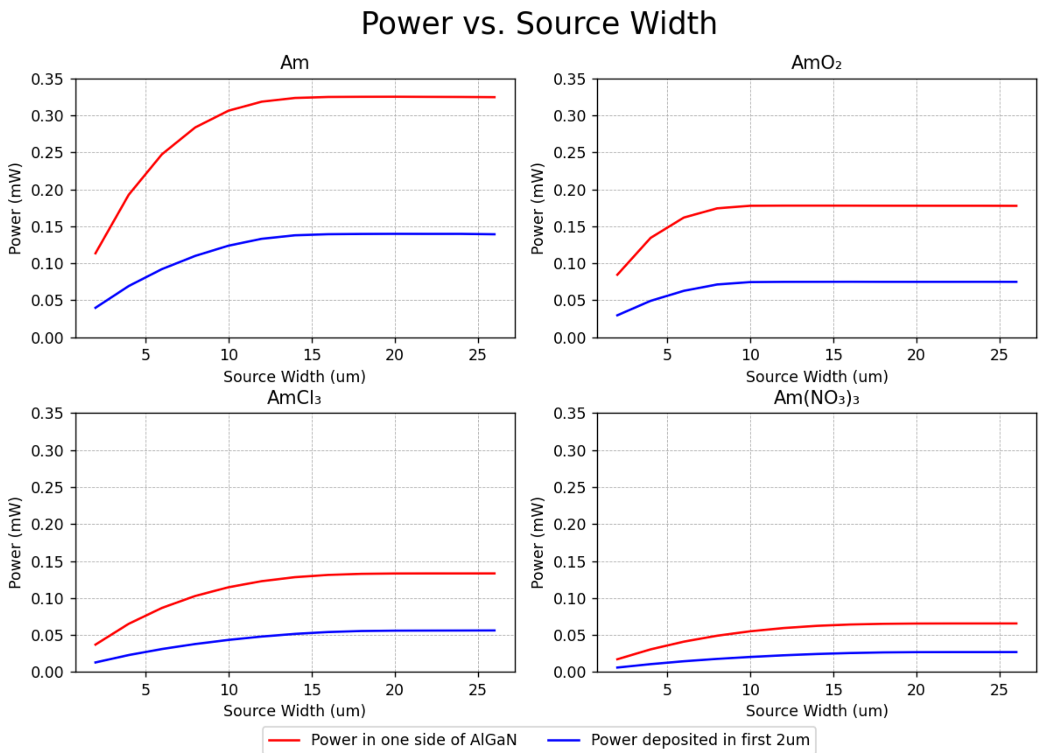

Figure 7. Power deposited in one side of the AlGaN (red) and first 2 µm of the AlGaN (blue) shown for each radioisotope studied.

Self-shielding can prevent alphas from depositing energy into the target region. At a certain width, depending on the self-shielding properties of the radioisotope, alphas released from deep in the source do not have a long enough range to deposit energy in the AlGaN. The saturation width is the characteristic dimension at which 90% of the maximum power output was achieved. Beyond the saturation width, additional radioisotopes do not add significant electrical power output. Saturation width decreases as density increases with the exception of AmO_2. Saturation widths are displayed in Figure 8 and Table 1. Table 1 also includes the activity and power associated with the saturation widths for each Am format.

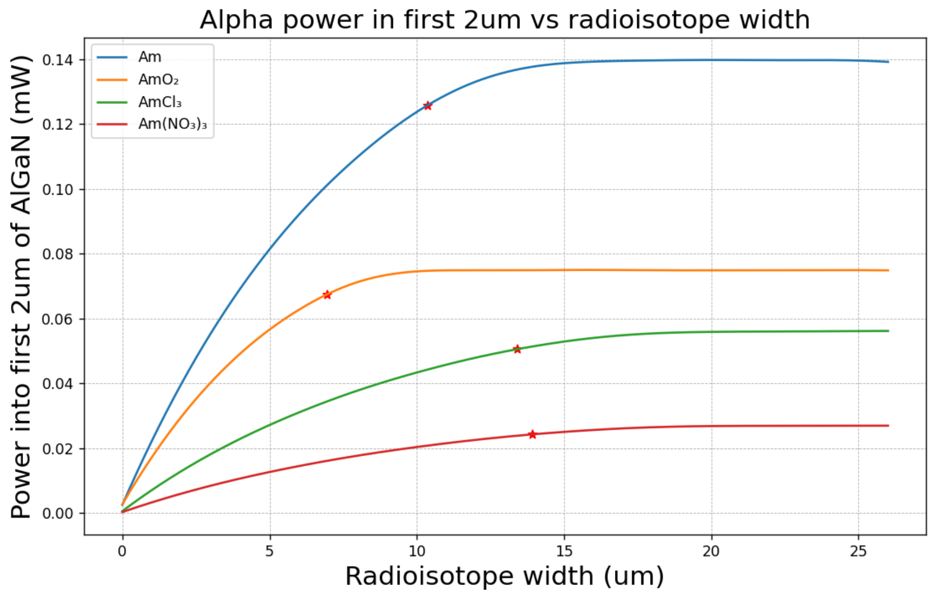

Figure 8. Power deposition in the first 2 µm of the AlGaN transducer as a function of radioisotope width for each Am compound studied. Saturation width and power are marked.

Table 1. 90% saturation width for each Am compound studied.

Radioisotope	Density (g/cc)	Specific activity (Ci/g)	90% saturation RI width (µm)	Power (2-µm AlGaN) (mW)	Activity (mCi)
Am	13.67	3.4	10.37	0.126	48.20
AmO_2	11.77	3.2	6.96	0.068	26.21
$AmCl_3$	5.87	2.5	13.41	0.051	19.68
$Am(NO_3)_3$	3.52	1.92	13.91	0.024	9.40

Note: Radioisotopes (RIs) are ordered from high to low density.

Once the optimal radioisotope width was calculated for each compound, the energy deposition in the first 2 µm (PIN junction) of the AlGaN was calculated. This result is useful for finding the EHP generation rate and can be used to optimize the dopant concentration and size of the P, I, and N regions. The power density is calculated using the power deposited in the first 2 µm divided by the mass or volume of a device with 10 µm (standard thickness) AlGaN on either side. Both gravimetric and volumetric power density (considering 10% conversion efficiency of power in the first 2 µm to usable electrical power) was then calculated for each compound and is displayed in Table 2.

Table 2. Double-sided AV device specifications based on 90% saturation width.

Radioisotope	Electrical power output (mW)	Power density (W/kg)	Power density (W/cc)	Net efficiency (%)	Activity (mCi)
Am	0.0272	1.035	8.968	1.73	48.20
AmO_2	0.0148	0.727	5.482	1.73	26.21
$AmCl_3$	0.0111	0.554	3.317	1.73	19.68
$Am(NO_3)_3$	0.0053	0.313	1.574	1.74	9.40

Notes: This model assumes 10% conversion efficiency of power deposited in the first 2 μm of the AlGaN to electrical power. The contribution of energy deposited is composed of 87% alpha energy and 13% secondary electron energy losses.

EHP generation calculation in an energy converter is needed for simulating the device physics in COMSOL. When EHPs are generated in the depletion zone, the build in electric field separates the charge carriers and creates a current, leading to usable electrical energy. To calculate the maximum possible EHP generation per particle, the following equation can be used:

$$G = E/(2.8\, E_g + 0.5\ eV)$$

where E_g is material bandgap (4 eV for AlGaN) (Spencer and Alam 2019). This value can be multiplied by the activity of the radioisotope to find the EHP generation rate (Table 3). This equation does not factor in all the loss mechanisms (i.e., optical phonon generation, bandgap losses, or thermalization losses) that manifest in the particle interactions in the AlGaN. To obtain an accurate model of the device, experimentation must be done to find the ratio of energy deposited from each loss mechanism.

Table 3. EHP generation rate in the first 2 μm of AlGaN.

Radioisotope	Am	AmO_2	$AmCl_3$	$Am(NO_3)_3$
Saturation width (μm)	10.37	6.96	13.41	13.91
Activity (mCi)	48.20	26.21	19.68	9.40
Max EHP generation rate in first 2 μm (s^{-1})	$7.27 \cdot 10^{13}$	$3.94 \cdot 10^{13}$	$2.96 \cdot 10^{13}$	$1.42 \cdot 10^{13}$
Max current (μA)	11.64	6.32	4.74	2.28

Notes: Shows ideal EHP generation given no losses. Only EHPs in the first 2 μm are likely to be collected and converted to electrical energy.

4. Conclusion

In this study, radioisotope width was optimized for power deposition in the first 2 μm of an AlGaN converter for ^{241}Am foil, AmO_2, $AmCl_3$, and $Am(NO_3)_3$. Performance metrics and EHP generation rates were calculated for these devices. Further optimization of doping concentration and PN or PIN layer thickness will be conducted for an accurate analysis of this device. These Am compounds can be coupled with AlGaN, a high-radiation–resistant energy converter that can withstand the 5.5-MeV alpha particles released, resulting in a prolonged lifetime.

Although pure Am in foil format showed the highest power deposition (0.126 mW) in the first 2 μm of AlGaN, it would be difficult to manufacture an Am foil as thin as 10.37 μm to achieve the 90% saturation width in a real AV device. AmO2 is the radioisotope compound that generated the next highest saturation power at 0.0148mW and can be accurately deposited on AlGaN in a 6.96μm layer.

It should be noted that utilizing a 10um layer of AmCl3 instead of Am-nitrate will result in a factor of 2x increase in calculated electrical power. This comes about from the fact that the specific activity increases by 30% in of AmCl3 vs Am(NO3)3. Secondly, the increase in activity for the equivalent 10um layer increases by a factor of 2.1. Together this supports the use of AmCl3 if possible.

For future studies, it is observed that AmO_2 does not follow the trend of decreasing source efficiency with increasing density. We will investigate the possibility that the oxygen chemical bond strength contributes to increased self-absorption.

A separate set of simulations were conducted comparing diamond—another high-radiation–tolerant semiconductor with high electron mobility—to AlGaN. It was shown that the penetration range of 5.5-MeV alphas emitted from ^{241}Am had a range of 15 and 11 μm for alphas and electrons, respectively, in diamond. This compares to 10.2 and 3.7 μm for alphas and electrons, respectively, in AlGaN.

The 90% saturation thicknesses ^{241}Am layer shown in Table 1 (<15 μm) can be paired with a cesium iodide (CsI) scintillator. A 5.5-MeV alpha is stopped within 50 μm of the CsITl scintillator. An indium gallium phosphide (InGaP) electronic lift-off energy converter reduces the typical solar cell of thickness from 1 mm to 30 μm (Figure 9). With these technical modifications, reducing the overall device thickness to a less than 175-μm-thick alphaphotovoltaic (APV) device is a realistic design for future versions.

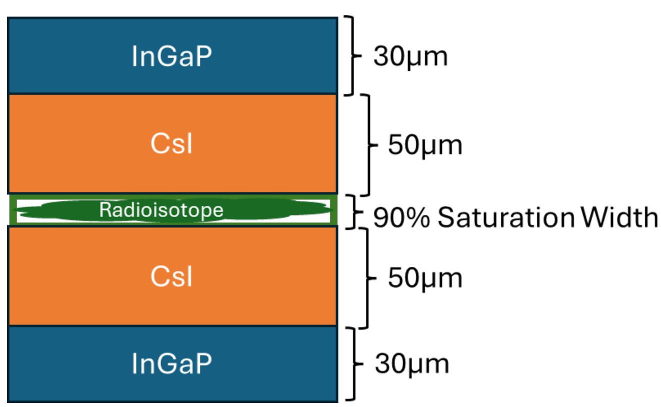

Figure 9. Schematic design of APV device <175 μm thick.

5. References

Olsen LC. Review of betavoltaic energy conversion. National Aeronautics and Space Administration (US); 1993 May. NASA Conference Publication. p. 256–256.

Prelas MA et al. A review of nuclear batteries. Prog Nucl Energy. 2014;75:117–148.

Spencer MG, Alam T. High power direct energy conversion by nuclear batteries. Appl Phys Rev. 2019;6(3).

Van de Walle CG, Stampfl C, Neugebauer J, McCluskey MD, Johnson NM. Doping of AlGaN alloys. MRS Internet J Nitride Semicond Res. 1999; 4(Suppl 1):890–901.

Weaver BD, Martin PA, Boos JB, Cress CD. Displacement damage effects in AlGaN/GaN high electron mobility transistors. IEEE Trans Nucl Sci. 2012; 59(6):3077–3080.

Weaver BD et al. On the radiation tolerance of AlGaN/GaN HEMTs. ECS J Solid State Sci Technol. 2016;5(7):Q208.

Appendix A. Monte-Carlo N Particle (MCNP) Input Deck of 10-µm-thick Americium (Am) Source

The following MCNP input deck models an Am foil of 10-µm-thick layer emitting alpha particles of 5.5 MeV. The isotropic emission is captured by AlGaN regions modelling an energy converter.

Model of 1 × 1-cm volumetric Am source into AlGaN.

```
c ------------------------------------------------------------------------
c
c +------------------------------------------------------+
c |                                                      |
c |                            Cell Cards                |
c |                                                      |
c +------------------------------------------------------+
c # mat  density  surface    data
 2 4  -6.07   -2  imp:e,a 1 u=1  $AlGaN layer
 3 4  -6.07   -3  imp:e,a 1 u=1  $AlGaN layer
 4 4  -6.07   -4  imp:e,a 1 u=1  $AlGaN layer
 5 4  -6.07   -5  imp:e,a 1 u=1  $AlGaN layer
 6 4  -6.07   -6  imp:e,a 1 u=1  $AlGaN layer
 7 4  -6.07   -7  imp:e,a 1 u=1  $AlGaN layer
 8 4  -6.07   -8  imp:e,a 1 u=1  $AlGaN layer
 9 4  -6.07   -9  imp:e,a 1 u=1  $AlGaN layer
 10 4  -6.07   -10  imp:e,a 1 u=1  $AlGaN layer
 11 4  -6.07   -11  imp:e,a 1 u=1  $AlGaN layer
 12 4  -6.07   -12  imp:e,a 1 u=1  $AlGaN layer
 17 3  -13.67  -17  imp:e,a 1 u=1  $Am
 18 4  -6.07   -18  imp:e,a 1 u=1  $AlGaN top layer
c air encasing
23 2    -0.00129    -23 2 3 4 5 6 7 8 9 10 11 12 17 18 imp:e,a 1 u=1
24 0 23              imp:e,a 1 u=1
c room
25 2  -0.00129  -24    imp:e,a 1 fill=1
26 0        24    imp:e,a 0    $outside world

c +------------------------------------------------------+
c |                                                      |
c |                         Surface Cards                |
c |                                                      |
c +------------------------------------------------------+
c # type param
2  rpp -0.5 0.5 -0.5 0.5 -0.0002 +0     $AlGaN layers 100nm
3  rpp -0.5 0.5 -0.5 0.5 -0.0004 -0.0002  $AlGaN layers 100nm
4  rpp -0.5 0.5 -0.5 0.5 -0.0006 -0.0004  $AlGaN layers 100nm
5  rpp -0.5 0.5 -0.5 0.5 -0.0008 -0.0006  $AlGaN layers 100nm
6  rpp -0.5 0.5 -0.5 0.5 -0.0010 -0.0008  $AlGaN layers 100nm
7  rpp -0.5 0.5 -0.5 0.5 -0.0012 -0.0010  $AlGaN layers 100nm
8  rpp -0.5 0.5 -0.5 0.5 -0.0014 -0.0012  $AlGaN layers 100nm
9  rpp -0.5 0.5 -0.5 0.5 -0.0016 -0.0014  $AlGaN layers 100nm
10 rpp -0.5 0.5 -0.5 0.5 -0.0018 -0.0016  $AlGaN layers 100nm
11 rpp -0.5 0.5 -0.5 0.5 -0.0020 -0.0018  $AlGaN layers 100nm
12 rpp -0.5 0.5 -0.5 0.5 -0.0022 -0.0020  $AlGaN layers 100nm
17 rpp -0.5 0.5 -0.5 0.5  0   +0.0010  $Am10 um MATHCH W/SDEF
18 rpp -0.5 0.5 -0.5 0.5 +0.0010  +0.0032 $AlGaN top layer
c air to encase AlGaN
```

```
23  rpp -.6 .6  -.6 .6  -.0050 .0061  $encasing air .0029 more than top
c room dimensions
24  rpp -.62 .62 -.62 .62 -.0052 .0063 $room air

c +-------------------------------------------------------+
c |                                                       |
c |                  Material Cards                       |
c |                                                       |
c +-------------------------------------------------------+
c m# isotope percent  &(newline)    $comment
 m2  8016.03e  .3   7014.03e  .7      $air   0.00129 g /cc
 m3  95000.03e  1                $Am
 m4  13000.03e  1  31000.03e 1 7014.03e  1    $AlGaN 6.07 g/cc
c +-------------------------------------------------------+
c |                                                       |
c |                  Source Definition                    |
c |                                                       |
c +-------------------------------------------------------+
c Rectangular volumetric source. MATCH W/SURFACE CARD
c
SDEF X=d1 Y=d2 Z=d3 Par=A ERG=5.5
SI1 -0.5 0.5 $ X span
SP1 0 1
SI2 -0.5 0.5 $ y span
SP2 0 1
SI3 0 0.0010 $ Z span: source thickness
SP3 0 1
c +-------------------------------------------------------+
c |           Data Cards                                  |
c +-------------------------------------------------------+
 mode E A
 DBCN 17J 2  $Originally DBCN 17J 2 default
 PHYS:E 14J 1.0e-5 $Original is 1keV change 10eV to 1keV
c PHYS:A 10 3J 0 J 1 0.65 2J 0 0 0 0.917 J J 1e-3
  PHYS:A 10 3J 0 J 1 0.65 2J 0 0 0 0.917 J 0 1e-3
c changed J to 0 and changed drp cuttoff to default of 20 keV page 333
c PHYS:P 100 0 0 0 0 J 0
 cut:E j 1.0e-3 $1keV low energy cutoff change to 1.0e-3 next
c cut:P j 1.0e-6 $1keV
 cut:A j 1e-2
nps 250000
c +-------------------------------------------------------+
c |                                                       |
c |                    Tallies                            |
c |                                                       |
c +-------------------------------------------------------+
c reported in order of number 4, 6, 14, 16
fc6 Adep in cell MeV/g
 f6:a 2 3 4 5 6 7
 e6 0 198i 5.5
fc16 Adep in cell MeV/g
  f16:a 8 9 10 11 12
  e16 0 198i 5.5
fc26 Adep in cell MeV/g
  f26:a 17 18 23
```

```
  e26 0 198i 5.5
fc4 Aflux in cell particles/cm^2
 f4:a 2 3 4 5 6 7 8 9 10 11 12 17 18 23
 e4 0 198i 5.5
fc36 edep in cell MeV/g
  f36:e 2 3 4 5 6 7
  e36 0 198i 0.003
 fc46 edep in cell MeV/g
  f46:e 8 9 10 11 12
  e46 0 198i 0.003
 fc56 edep in cell MeV/g
  f56:e 17 18 23
  e56 0 198i 0.003
fc14 eflux in cell particles/cm^2
 f14:e 2 3 4 5 6 7 8 9 10 11 12 17 18 23
c 2 3 6 9 12 15 23
 e14 0 198i 0.003
c +-------------------------------------------------------+
c |                                                       |
c |                     Mesh                              |
c |                                                       |
c +-------------------------------------------------------+
c
tmesh
c
c (a)radial meshes (b)zaxis(symmetry) (c)angles counterclockwise
c
c flux=#/cm2   $dose=rem/hr  $pedep=MeV/cm3
c
c flux: flux
c pedep: total energy deposition/unit vol
c dose: dose over cross planes
 rmesh21:a flux pedep
c depth profile NOX
 cora21  -0.6      0.6
 corb21  -0.6  68i  0.6
 corc21  -.003 198i  0.0040
c
rmesh31:e flux pedep
c depth profile NOX
 cora31  -0.6      0.6
 corb31  -0.6  68i   0.6
 corc31  -.003 198i 0.0040
endmd
```

Appendix B. Energy Deposition Tables

Tables B-1 through B-4 in this appendix were created from the master sheets of Monte-Carlo N Particle (MCNP) Run Log and Data.xlsx. There are four tables shown, one for the alpha data of each of the americium (Am) compounds studied. The energy deposited in AlGaN layers is compared to the radioisotope mass and activity as a function of radioisotope thickness.

Table B-1. Am alpha data.

RI Thickness (u	RI Mass (g)	Activity (mCi	Activity (decay	one side of SC (MeV)	both sides of SC (MeV)	in radioisotope (MeV)	Energy into first 2um (MeV)	Source Efficiency (both sides) (%	Source Power (mW)	Power into one side of SC (m	Power into both sides of SC (m	in radioisotope (mW)	Power into first 2um (mW)
2	2.73E-03	9.38	3.47E+08	2.04	4.07	0.68	0.72	74.0%	0.31	1.13E-01	0.23	0.04	3.982E-02
4	5.47E-03	18.76	6.94E+08	1.73	3.46	1.18	0.62	62.8%	0.61	1.93E-01	0.38	0.13	6.921E-02
6	8.20E-03	28.13	1.04E+09	1.48	2.96	1.59	0.55	53.8%	0.92	2.47E-01	0.49	0.26	9.213E-02
8	1.09E-02	37.51	1.39E+09	1.28	2.55	1.94	0.49	46.3%	1.22	2.84E-01	0.57	0.43	1.100E-01
10	1.37E-02	46.89	1.73E+09	1.10	2.20	2.25	0.45	40.0%	1.53	3.06E-01	0.61	0.62	1.238E-01
12	1.64E-02	56.27	2.08E+09	0.95	1.91	2.51	0.40	34.6%	1.83	3.18E-01	0.64	0.84	1.331E-01
14	1.91E-02	65.64	2.43E+09	0.83	1.66	2.74	0.35	30.2%	2.14	3.23E-01	0.65	1.06	1.378E-01
16	2.19E-02	75.02	2.78E+09	0.73	1.46	2.92	0.31	26.5%	2.45	3.25E-01	0.65	1.30	1.393E-01
18	2.46E-02	84.40	3.12E+09	0.65	1.30	3.07	0.28	23.6%	2.75	3.25E-01	0.65	1.54	1.396E-01
20	2.73E-02	93.78	3.47E+09	0.58	1.17	3.19	0.25	21.2%	3.06	3.25E-01	0.65	1.77	1.398E-01
22	3.01E-02	103.15	3.82E+09	0.53	1.06	3.29	0.23	19.3%	3.36	3.25E-01	0.65	2.01	1.397E-01
24	3.28E-02	112.53	4.16E+09	0.49	0.97	3.37	0.21	17.7%	3.67	3.25E-01	0.65	2.25	1.397E-01
26	3.55E-02	121.91	4.51E+09	0.45	0.90	3.44	0.19	16.3%	3.97	3.25E-01	0.65	2.48	1.392E-01

Table B-2. AmO_2 alpha data.

RI Thickness (u	RI Mass (g)	Activity (mCi	Activity (decay	one side of SC (MeV)	both sides of SC (MeV)	in radioisotope (MeV)	Energy into first 2um (MeV)	Source Efficiency (both sides) (%	Source Power (mW)	Power into one side of SC (m	Power into both sides of SC (m	in radioisotope (mW)	Power into first 2um (mW)
2	0.00	7.53	2.79E+08	1.89	3.77	1.10	0.66	68.6%	0.25	8.45E-02	0.17	0.05	2.9673E-02
4	0.00	15.07	5.57E+08	1.50	3.00	1.83	0.55	54.6%	0.49	1.34E-01	0.27	0.16	4.9188E-02
6	0.01	22.60	8.36E+08	1.21	2.41	2.40	0.47	43.9%	0.74	1.62E-01	0.32	0.32	6.2744E-02
8	0.01	30.13	1.11E+09	0.98	1.95	2.85	0.40	35.4%	0.98	1.74E-01	0.35	0.51	7.1299E-02
10	0.01	37.66	1.39E+09	0.80	1.59	3.19	0.33	28.9%	1.23	1.78E-01	0.35	0.71	7.4563E-02
12	0.01	45.20	1.67E+09	0.66	1.33	3.45	0.28	24.1%	1.47	1.78E-01	0.36	0.92	7.4878E-02
14	0.02	52.73	1.95E+09	0.57	1.14	3.64	0.24	20.7%	1.72	1.78E-01	0.36	1.14	7.4933E-02
16	0.02	60.26	2.23E+09	0.50	0.99	3.77	0.21	18.1%	1.96	1.78E-01	0.36	1.35	7.5007E-02
18	0.02	67.80	2.51E+09	0.44	0.88	3.88	0.19	16.1%	2.21	1.78E-01	0.36	1.56	7.4907E-02
20	0.02	75.33	2.79E+09	0.40	0.80	3.97	0.17	14.5%	2.46	1.78E-01	0.35	1.77	7.4890E-02
22	0.03	82.86	3.07E+09	0.36	0.72	4.04	0.15	13.1%	2.70	1.78E-01	0.35	1.98	7.4905E-02
24	0.03	90.39	3.34E+09	0.33	0.66	4.10	0.14	12.0%	2.95	1.78E-01	0.35	2.20	7.4953E-02
26	0.03	97.93	3.62E+09	0.31	0.61	4.15	0.13	11.1%	3.19	1.78E-01	0.35	2.41	7.4878E-02

Table B-3. $AmCl_3$ alpha data.

RI Thickness (u	RI Mass (g)	Activity (mCi	Activity (decay	one side of SC (MeV)	both sides of SC (MeV)	in radioisotope (MeV)	Energy into first 2um (MeV)	Source Efficiency (both sides) (%	Source Power (mW)	Power into one side of SC (m	Power into both sides of SC (m	in radioisotope (mW)	Power into first 2um (mW)
2	1.17E-03	2.94E+00	1.09E+08	2.13	4.24	0.66	0.74	77.1%	0.10	3.70E-02	0.07	0.01	1.2921E-02
4	2.35E-03	5.87E+00	2.17E+08	1.87	3.73	1.14	0.66	67.9%	0.19	6.52E-02	0.13	0.04	2.2899E-02
6	3.52E-03	8.81E+00	3.26E+08	1.66	3.31	1.54	0.60	60.2%	0.29	8.66E-02	0.17	0.08	3.1059E-02
8	4.70E-03	1.17E+01	4.34E+08	1.48	2.95	1.89	0.54	53.6%	0.38	1.03E-01	0.21	0.13	3.7829E-02
10	5.87E-03	1.47E+01	5.43E+08	1.32	2.63	2.19	0.50	47.8%	0.48	1.15E-01	0.23	0.19	4.3364E-02
12	7.04E-03	1.76E+01	6.52E+08	1.18	2.35	2.46	0.46	42.7%	0.57	1.23E-01	0.25	0.26	4.7943E-02
14	8.22E-03	2.05E+01	7.60E+08	1.05	2.10	2.70	0.42	38.2%	0.67	1.28E-01	0.26	0.33	5.1507E-02
16	9.39E-03	2.35E+01	8.69E+08	0.94	1.88	2.91	0.39	34.2%	0.77	1.31E-01	0.26	0.41	5.4033E-02
18	1.06E-02	2.64E+01	9.77E+08	0.85	1.69	3.10	0.35	30.7%	0.86	1.33E-01	0.26	0.48	5.5418E-02
20	1.17E-02	2.94E+01	1.09E+09	0.77	1.53	3.26	0.32	27.8%	0.96	1.33E-01	0.27	0.57	5.5899E-02
22	1.29E-02	3.23E+01	1.19E+09	0.70	1.39	3.39	0.29	25.3%	1.05	1.33E-01	0.27	0.65	5.6007E-02
24	1.41E-02	3.52E+01	1.30E+09	0.64	1.27	3.50	0.27	23.2%	1.15	1.33E-01	0.27	0.73	5.6082E-02
26	1.53E-02	3.82E+01	1.41E+09	0.59	1.18	3.60	0.25	21.4%	1.24	1.33E-01	0.266	0.81	5.6177E-02

Table B-4. $Am(NO_3)_3$ alpha data.

RI Thickness (	RI Mass (g	Activity (mC	Activity (decay	one side of SC (MeV)	both sides of SC (MeV)	in radioisotope (MeV)	Energy into first 2um (MeV)	Source Efficiency (both sides) (	Source Power (mW)	Power into one side of SC (m	Power into both sides of SC (m	in radioisotope (mW)	Power into first 2um (mW)
2	7.04E-04	1.35E+00	5.00E+07	2.15	4.29	0.68	7.48E-01	77.9%	0.04	1.72E-02	0.03	0.01	5.992E-03
4	1.41E-03	2.70E+00	1.00E+08	1.91	3.81	1.16	6.65E-01	69.2%	0.09	3.06E-02	0.06	0.02	1.066E-02
6	2.11E-03	4.06E+00	1.50E+08	1.71	3.41	1.57	6.04E-01	61.9%	0.13	4.10E-02	0.08	0.04	1.451E-02
8	2.82E-03	5.41E+00	2.00E+08	1.53	3.05	1.92	5.53E-01	55.5%	0.18	4.91E-02	0.10	0.06	1.773E-02
10	3.52E-03	6.76E+00	2.50E+08	1.37	2.74	2.23	5.09E-01	49.9%	0.22	5.51E-02	0.11	0.09	2.038E-02
12	4.22E-03	8.11E+00	3.00E+08	1.24	2.47	2.51	4.70E-01	44.9%	0.26	5.94E-02	0.12	0.12	2.258E-02
14	4.93E-03	9.46E+00	3.50E+08	1.11	2.22	2.76	4.34E-01	40.4%	0.31	6.24E-02	0.12	0.15	2.434E-02
16	5.63E-03	1.08E+01	4.00E+08	1.00	2.00	2.98	4.00E-01	36.4%	0.35	6.42E-02	0.13	0.19	2.564E-02
18	6.34E-03	1.22E+01	4.50E+08	0.90	1.80	3.18	3.67E-01	32.8%	0.40	6.52E-02	0.13	0.23	2.648E-02
20	7.04E-03	1.35E+01	5.00E+08	0.82	1.63	3.35	3.35E-01	29.7%	0.44	6.55E-02	0.13	0.27	2.683E-02
22	7.74E-03	1.49E+01	5.50E+08	0.74	1.49	3.49	3.05E-01	27.0%	0.48	6.56E-02	0.13	0.31	2.691E-02
24	8.45E-03	1.62E+01	6.00E+08	0.68	1.36	3.62	2.80E-01	24.8%	0.53	6.56E-02	0.13	0.35	2.693E-02
26	9.15E-03	1.76E+01	6.50E+08	0.63	1.26	3.72	2.59E-01	22.9%	0.57	6.56E-02	0.13	0.39	2.696E-02

List of Symbols, Abbreviations, and Acronyms

AlGaN	aluminum gallium nitride
Am	americium
$AmCl_3$	americium(III) chloride
$Am(NO_3)_3$	americium(III) nitrate
AmO_2	americium dioxide
APV	alphaphotovoltaic
AV	alphavoltaic
CsI	cesium iodide
EHP	electron hole pair
GaN	gallium nitride
HEMT	High Electron Mobility Transistor
InGaP	indium gallium phosphide
MCNP	Monte-Carlo N Particle
Mg	magnesium
RI	radioisotope
Si	silicon
SiC	silicon carbide
SRIM	Stopping Range in Matter

1 (PDF)	DEFENSE TECHNICAL INFORMATION CTR DTIC OCA
1 (PDF)	DEVCOM ARL FCDD RLB CI TECH LIB